Application of a Quasi in-situ Experimental Approach to Estimate 3-D Pitting Corrosion Kinetics in Stainless Steel

DOI:
10.1149/2.0381613jes

Document Version
Accepted author manuscript

Journal of The Electrochemical Society, **163** (13) C1-C7 (2016)
0013-4651/2016/163(13)/C1/7/$33.00 © The Electrochemical Society

Application of a Quasi In Situ Experimental Approach to Estimate 3-D Pitting Corrosion Kinetics in Stainless Steel

F. A. Almuaili,[a,z] S. A. McDonald,[b] P. J. Withers,[b] and D. L. Engelberg[a]

[a]*Corrosion and Protection Centre, School of Materials, The University of Manchester, Manchester M13 9PL, United Kingdom*
[b]*Manchester X-ray Imaging Facility, School of Materials, The University of Manchester, Manchester M13 9PL, United Kingdom*

Pitting corrosion kinetics of type 304L stainless steel have been obtained using a quasi in-situ X-ray computed tomography (X-ray CT) approach. A miniature electro-chemical cell was constructed to allow imaging during potentio-dynamic polarization of a wire specimen. The formation of three discrete pits was observed, allowing comparison between real pit geometry and different geometrical assumptions to estimate pit growth kinetics. The pit volumes obtained by X-ray CT showed good fit with the volume of metal dissolution calculated using Faraday's law. Large fluctuations of the mean current density were observed during the pit nucleation stage, followed by pit growth with mean current densities of 1–3 A.cm^{-2}. Stability products associated with these pits were on the order of 0.3–0.6 A.m^{-1}, with diffusivity parameter (D.ΔC) of 1.68–3.04 × 10^{-8} mol.cm^{-1}.s^{-1}. Diffusion coefficients for stable pit growth of 0.83–0.96 × 10^{-5} cm^2.s^{-1} were estimated for metal ion concentrations of 4.2 M.

Manuscript submitted February 23, 2016; revised manuscript received September 8, 2016. Published 00 0, 2016.

Pitting or crevice corrosion can occur on stainless steels exposed to halide containing environments. The breakdown of the passive surface film results in the nucleation of local attack, which is followed by pit growth, with a number of mechanisms proposed for each stage.[1,2] Electrochemical polarisation above the critical pitting potential leads to nucleation of pits, in the form of localised metal dissolution, with corrosive electrolyte developing inside the nucleated pit due to hydrolysis of dissolved metal ions, and chloride ions being attracted from bulk solution to maintain charge neutrality.[3] At high applied electrochemical potentials, pits grow with a polished inner surface morphology, associated with salt film formation, whereas pits grown at lower applied potentials display more irregular etch morphologies of the internal pit surface.[4] An undercutting mechanism was suggested for pit growth at high electrochemical potentials, leading to the development of dish shaped pits covered by metal lacy covers.[5–10]

Pit propagation is controlled by diffusion of species through the salt film at the inner surface of pits. A high anodic dissolution rate, which facilitate critical ion concentrations inside a pit, is criterion for pits to propagate.[11] The anolyte concentration inside a pit influences pit growth kinetics and the pit shape. For example, a 3 M concentration of dissolved metal ions was proposed as minimum concentration to turn an open hemispherical meta-stable pit into a stable pit. However, pits developed with lacy metal covers grow at far lower metal ion concentrations, since these covers are believed to provide an effective diffusion barrier[12] and an increased ohmic resistance between pit interior and the bulk electrolyte.[1] Based on these observations for the transition between meta-stable and stable pits, the "pit stability product" (0.3 A. m^{-1} ≤ i.r ≤ 0.6 A. m^{-1}) was proposed, with the latter based on the evolution of pit current density (i) and pit depth (r).[12]

To sustain stable pit growth under anodic polarisation, a minimum current density is required, with typical values for stainless steel in the region of 1–5 A.cm^{-2}.[13,14] For pit initiation, however, far higher current densities were observed, followed by a reduction with increasing pit volume which corresponds to an increase in active pit surface area over time. The electrochemical potential at the pit bottom remains above the repassivation potential resulting in active dissolution conditions. Therefore, initial pit growth studies suggested that associated kinetics were potential dependent under charge transfer control, resulting in a hemispherical pit shape. After the formation of a salt film inside the pit due to limited solubility of cations, pit propagation is considered to be under diffusion-control and potential independent, where the pit shape changes into more elongated dish shape over time. The sides of the pit, typically referred to as lobes, grow faster than the bottom part. Furthermore, due to this mechanism the pit ratio (depth vs. width) can change, suggesting that pits grow in depth occurs under diffusion control, with ohmic resistance controlling lateral pit growth.[7] Typical current densities between 1–2 A.cm^{-2} are related to the precipitated salt film at the bottom of the pit, whereas, salt film free regions (side walls) show a maximum current in the range of 3–5 A.cm^{-2}.[9]

The growth kinetics of a single pit in type 304 stainless steel under potentiostatic polarisation control in 1 M NaCl with 0.4 M Na-thiosulfate solution showed parabolic behavior.[15] Pit volumes measured by means of mechanical grinding and sectioning followed by optical microscopy showed a good fit with the dissolved volume determined by current measurements using Faraday's law and assuming a hemispherical pit shape. The study also showed that pit growth under potentiostatic control in 3.5% wt NaCl and seawater was similar to pits grown under open circuit conditions in 1 M $FeCl_3$ solution, both indicating an exponential relation of pit growth with time.[16]

One dimensional (1-D) pit growth investigations using pencil electrodes[26] and two-dimensional (2-D) pit geometry estimated using thin foils and in-situ recording or radiography images[9] have been used to allow estimation of pit stability product. These methods allow pits underneath the metal surface to be observed, but the developed pit shape does not necessarily represent pit growth in 3-D. The effect of constraining pits to grow in 1-D or 2-D may not accurately reflect 3-D growth kinetics. It may affect transport processes of dissolved metal ions between pit anolyte and the bulk solution, which can subsequently affect local pit chemistry and associated growth dynamics.

For pencil electrode (1-D) measurements, pit growth occurs in depth by maintaining a constant surface area related to the diameter of the pencil electrode[14,17,18]. These 1-D studies revealed transition of pit growth kinetics from ohmic/dissolution control to diffusion control at high potentials. A transition current density between both growth regimes in the region of 1–5 A.cm^{-2}, with the latter a function of the chloride concentration inside the pit, was also observed.[14] Potential step experiment with 1-D electrodes further revealed the effect of Cr content and solution chemistry on the dissolution and passivation kinetics, suggesting that salt film precipitation controls the metal dissolution rate.[18] The effect of electrolyte species also has a profound effect on pit growth kinetics with, for example, the addition of sulfate to NaCl environment significantly reducing the current density for pit growth.[19] In this study, pit chemistry was determined based on the minimum concentration at the pit surface that maintains pit growth without passivation. The dissolved metal salt concentration was then estimated by assuming a constant diffusion coefficient (D), yielding diffusivity parameters (D.ΔC) of 3–3.5 × 10^{-8} mol.cm^{-1}.s^{-1} for NaCl, and 2 × 10^{-8} mol.cm^{-1}.s^{-1} for NaCl with sulfate.[19] Pistorius and Burstein also reported a reduction of current density in presence of sulfate for stable pitting on type 304 stainless steel.[20]

[z]E-mail: fahd.almuaili-2@postgrad.manchester.ac.uk

The development of pit shape and current density over time was recently obtained in stainless steel foils using in-situ X-ray synchrotron radiography experiments.[25] This study showed that an elongated dish-shape developed under potentiostatic control, with the pit shape remaining near-hemispherical under galvanostatic control. Current densities measured, based on pit boundary movement over time using a sequence of 2-D radiography images, showed that the distribution of current density along the pit perimeter was not uniform and was influenced by concentration of metal cations and the pit shape. Therefore higher values of current density at active lobes drive the pit growth through an undercutting process. Furthermore, the smooth surface at the bottom of the pits show lower current density, while the pit surface near the bulk solution tend to passivate. Pit growth showed fluctuation of the mean pit stability product with values between 0.3 and 0.4 $A.m^{-1}$ or above.[25] Pit diffusivity parameters ($D.\Delta C$) for 2-D pit growth in 0.1 M NaCl was estimated from the gradient between square depth and time, resulting in values of $1.05–2.6 \times 10^{-8}$ $mol.cm^{-1}s^{-1}$ under potentiostatic control, and $1.59–2.29 \times 10^{-8}$ $molcm^{-1}s^{-1}$ under galvanostatic control. For 1-D pit growth in 1 M NaCl a diffusivity parameters of 4.36×10^{-8} $molcm^{-1}s^{-1}$ was determined, with the difference attributed to the perforation factor between open pit (1-D) and covered pit (2-D).[9]

Corrosion pits initiated at the tip of a Type 304 stainless steel pin using a capillary micro-cell have also been observed in 3-D using X-ray synchrotron micro-tomography. Pits grown under current and potential control in 1 M NaCl electrolyte showed similar pit morphologies as reported in earlier 2-D pit growth studies on foils.[8] Another 3-D X-ray micro-tomography study was conducted recently, to investigate the relationship between pitting corrosion and intergranular corrosion in sensitised type 316H stainless steel exposed to 0.1 M NaCl electrolyte.[27] The results showed the occurrence of both forms of corrosion attack. Pits nucleated at the surface of the electo-chemically polarised wire, with the aggressive pit anolyte leading to intergranular attack along grain boundaries within the pit. Earlier 3-D studies also investigated the propagation of intergranular corrosion and stress corrosion cracking in sensitised austenitic stainless steel and aluminum alloy 5083, highlighting the application of 3D imaging on corrosion and crack growth kinetics.[28–30]

The aim of our study was to develop an experimental methodology to investigate 3D pitting corrosion kinetics during exposure to bulk electrolyte, by using a miniature 3-electrode electrochemical cell combined with quasi in-situ X-ray computed tomography (X-ray CT). The second goal was to obtain 3D pit growth kinetics, and compare those to literature reports of pit growth in 2D and 3D, obtained from experiments using miniature capillary probes.

Experimental

A solution annealed type 304L stainless steel wire with a diameter of 500 μm was used in this study, with a chemical composition of (wt%) 18.4 Cr, 8.7 Ni, 0.02 C, 1.4 Mn, 0.34 Si, 0.04 N, 0.03 P and 0.001 S. Short wire sections of 70 mm were cut and manually ground using 1200 grit SiC paper, followed by a rinse in deionised water. The surface of the wire was coated with beeswax exposing a cylindrical surface area of 2.83 mm^2.

The wire section was mounted vertically in a miniature electrochemical cell shown in Figure 1a, and the set-up was then placed in a ZEISS Xradia Micro tomography instrument (Figure 1b). The diameter of the cell was 24 mm, consisting of a lower part containing the electrolyte with a volume of approximately 9 ml for electrochemical polarisation measurements, and an upper part with a straining rig for applying a tensile load along the length of the wire. The latter was used in another study to investigate the effect of strain on pit growth kinetics and for assessing the nucleation of stress corrosion cracking. The bottom part of the cell housed a miniature reference electrode (Ag/AgCl, 3 M NaCl) and a miniature platinum counter electrode. Electrochemical polarisation tests were performed with a scan rate of 1 mV/s in aerated 0.1 M NaCl solution using an Ivium Potentiostat. Prior to polarisation, the open circuit potential (OCP) was monitored for 15 min. The current response was recorded during the polarisation experiment at a rate of 1 Hz.

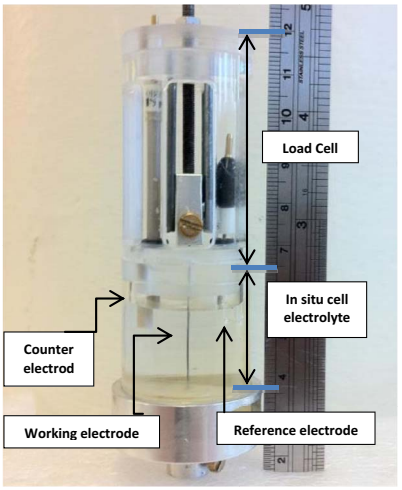

(a)

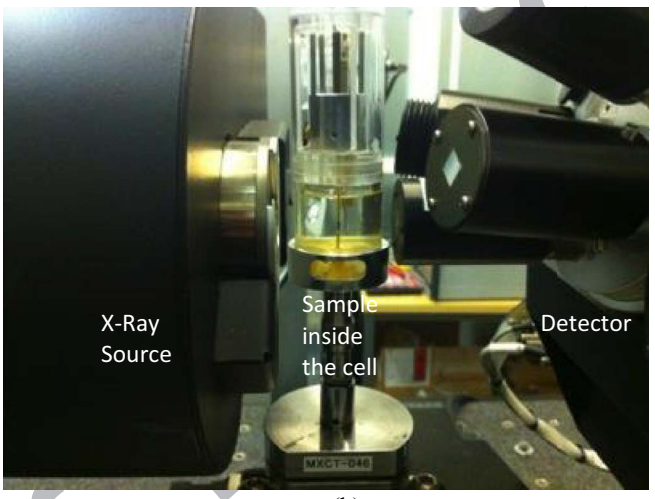

(b)

Figure 1. (a) Photo of the miniature electrochemical cell with capability to apply strain for in-situ X-ray tomography experiments with a type 304 L wire sample, (b) in-situ cell during an X-ray CT experiment.

Table I gives a summary of the in-situ experiment with associated polarisation cycles. After each cycle, one X-ray CT scan was performed to visualise the progress of pitting corrosion over time. X-ray

Table I. Summary of in-situ electrochemical polarisation experiment.

Step	Polarisation Cycles
0	X-ray CT scan (reference / without electrolyte)
1	OCP measurement (15 min.)
2	Potentio-dynamic polarisation from OCP to 644 mV vs. Ag/AgCl
3	X-ray CT scan 1 at OCP
4	OCP measurement (5 min)
5	2nd potentio-dynamic polarisation from OCP to 2 644 mV vs. Ag/AgCl
6	X-ray CT scan 2 at OCP
7	OCP measurement (5 min)
8	3rd potentio-dynamic polarisation from OCP to 700 mV vs. Ag/AgCl
9	X-ray CT scan (3) at OCP

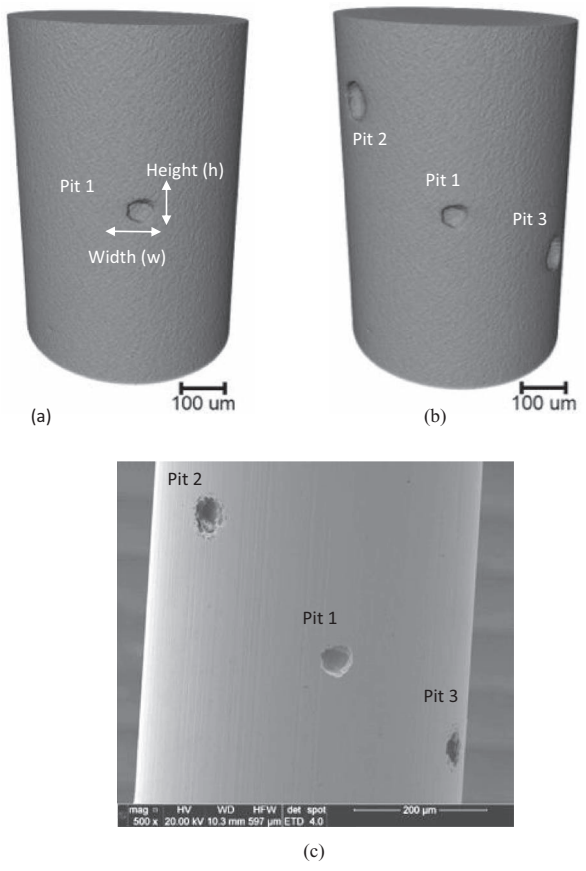

Figure 2. (a) Reconstructed X-ray CT data volume of the wire after the 1st electrochemical polarisation scan, (b) X-ray CT data volume after the 2nd potentio-dynamic polarisation cycle, and (c) SEM image of the wire sample with the three pits.

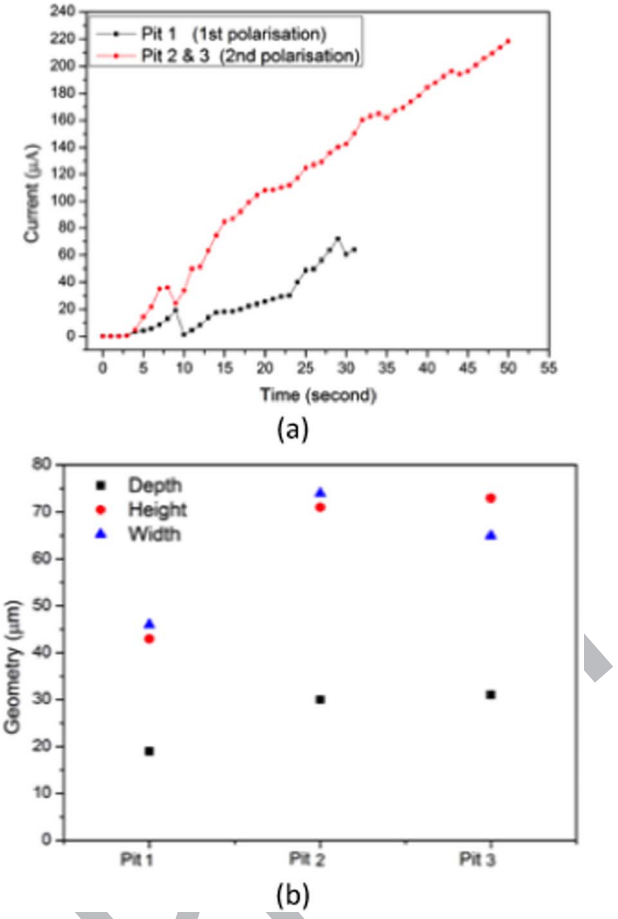

Figure 3. (a) Current evolution vs. time of the 1st and 2nd potentio-dynamic polarisation cycle with (b) measured depth (r), width (w) and height (h) of all three pits from X-ray CT data.

CT scans were recorded at OCP, with each scan taking approximately 2–3 hrs. The sample remained in the solution throughout the whole experiment. For the X-ray CT measurements an accelerating voltage of 120 kV was used, and 721 projections recorded with 2 × 2 binning. This resulted in a reconstructed voxel size of 1.83 µm, with a field of view of 2300 µm × 2300 µm.

The data was reconstructed using a Feldkamp-Davis-Kress (FDK) approach,[31] and images were segmented and visualised using Avizo software. After segmentation of each pit, the total volume, total pit surface area, pit depth, width, height, aspect ratio and shape were obtained. The pit depth, width and height were obtained by using 2-D slices of the 3-D data-set taken from the geometrical pit centre. This approach provided a snap-shot of pit dimensions after each polarisation cycle, with the current response recorded during the polarisation experiment providing in-situ pit growth information. The wire was then removed from the in-situ cell after step 9 (Table I), rinsed in water and images of the pits obtained using a FEI Quanta 650 scanning electron microscope (SEM).

Results and Discussion

The first X-ray CT scan (step 0) was recorded before the sample was exposed to the electrolyte, to obtain reference data of the investigated wire volume. This scan confirmed that no corrosion or mechanical damage (e.g. cracks) was present before the sample was polarised. After completing this scan, the NaCl electrolyte was introduced into the in-situ cell. The 1st potentio-dynamic polarisation (step 2 in Table I) resulted in the formation of one corrosion pit (pit 1), with the 2nd potentio-dynamic scan (step 5 in Table I) leading to the nucleation and growth of two new pits (pit 2 and 3). Figure 2a shows a 3-D view of the reconstructed tomography data of the wire with pit 1, and Figure 2b gives the same volume with all 3 pits, recorded after the 2nd polarisation cycle. The final polarisation cycle (step 8) did not result in the formation or further growth of corrosion pits. A SEM image of the wire after the test is shown in Figure 2c.

Electrochemical polarisation.—The OCP prior to the first polarisation was +129 mV vs Ag/AgCl (Step 1), with an OCP prior to the second scan of +151 mV (step 4). The current evolution over time of the first and second potentio-dynamic scan are shown in Figure 3a. During the first polarisation cycle, the current started to rise at +616 mV up to the applied max. potential of +644 mV vs. Ag/AgCl. The second polarisation resulted in a current increase starting at +596 mV but with a far steeper rise of current over time, resulting in approximately double the gradient compared to the current evolution observed during the first polarisation cycle. Both curves show a drop of current after a few seconds followed by a continuous rise again.

The shift in OCP after the first polarisation is either due to the growth of the passive surface film, often associated with anodic polarisation of passive material, or alternatively an effect of the high energy X-ray beam, causing chemical changes of the film/electrolyte interface. This shift is also observed after the second X-ray CT scan (step 6) with an OCP recorded of +178 mV vs. Ag/AgCl. A third polarisation cycle (step 7) was performed from OCP up to +700 mV, but no measurable current increase over time was observed. No further pit was nucleated during this cycle, which may be related to the limited number of active sites of inclusions at this potential.

Table II. Measured pit geometries.

	A-measured data from X-ray CT scans			B - depth measured by X-ray CT + assumption of a hemi-spherical pit shape			C- Faraday approach + assumption of a hemi-spherical pit shape		
Methods/pit parameters	Pit 1	Pit 2	Pit 3	Pit 1	Pit 2	Pit 3	Pit 1	Pit 2	Pit 3
Depth, r (μm)	19	30	31	19	30	31	**22.7***	**35.8***	**35.8***
Width, w (μm)	43	71	74	**38***	**60***	**62***	**45.4***	**71.6***	**71.6***
Height, h (μm)	46	73	65	**38***	**60***	**62***	**45.4***	**71.6***	**71.6***
Volume, V (μm^3)	25476	96039	97535	**14358***	**56520***	**62362***	24370	96265	96265
Surface area, A (μm^2)	3432	8058	8307	**2267***	**5652***	**6035***	**3225***	**8060***	**8060***

* assumed values in bold.

Pit geometry and estimation of growth kinetics.—The pit dimensions at the end of the polarisation with depth, width and height obtained from measurements of the X-ray CT data are shown in Figure 3b. All pit volume and surface parameters measured via segmentation are summarised in Table II. Beside the direct measurements from X-ray CT data, two additional geometrical approaches (B and C) were also explored to estimate pit growth kinetics. Table I lists the parameters of all 3 approaches, which were applied to simulate pit growth kinetics.

In approach A, all values were measured from segmented X-ray CT data. The area of the pit surface was obtained by measuring the surface area of the segmented pit volume, excluding the area of the pit mouth. This represented the real area of the pit internal surface assuming the pit cover is passive. In the case of pits 2 and 3, the similar size of both segmented volumes from X-ray CT data, in combination with the current evolution over time implied that both had nucleated at the same time during the 2nd polarisation scan. This assumption of simultaneous pit growth then allowed the current in Figure 3a to be equally divided between pit 2 and 3, which is supported by the observed current over time gradient, i.e. approximately double that observed for the growth of pit 1.

In approach B, the pit volume and surface area were calculated by assuming the pit shape is hemi-spherical with only the pit depth (r) obtained from the X-ray CT measurements. The computed volume (V) of the hemisphere followed the equation $V = 2/3.\pi.(r)$,[3] with the development of the surface area determined by assuming isotropic growth from a local initiation point at the centre of the hemi-sphere diameter. To determine evolution of pit surface area over time, it was assumed that pits were active at the end of the polarisation cycle. This is supported by the current response in Figure 3a. Assumption of symmetric growth of the pit volume then allowed back extrapolation of the pit surface area from the end of the polarisation scan to the point where the current started to rise. This assumption is based on a mean current density over the entire pit surface area to satisfy homogeneous growth of both, the pit surface area and pit volume. However, this also allowed comparison of the measured current response in Figure 3a, by computing the measured current over the estimated surface area for each point in time, shown as current density plots in Figures 4a and 4b. Comparison of the behavior of pits observed in this study then allowed trends of current density and associated stability product values over time to be identified (Figure 4).

In approach C, the pit volume was calculated from the charge passed during the period of pit growth in Figure 3a and converted into mass using Faraday's law. The metal dissolution assumed an average metal cation charge of $n = 2.19$, atomic weight $M = 55.79$ g.mol^{-1} and density of $\rho = 7.97$ g.cm^{-3}, and Faraday's constant $F = 96485$ coulomb/mol.[12] Also a hemispherical pit shape was assumed, with a radius based on the dissolved volume (Table II). The development of the pit surface area for estimating the corresponding current densities was also based on a homogeneous symmetric growth, as described for approach B. From the current-time response in Fig. 3a, the pit current density and pit stability product over time were estimated (Figure 4).

Table II indicates that pit volumes calculated via segmentation (approach A) are close to those calculated via Faraday's law (approach C), with a difference of less than 6%. This difference may be explained with uncertainty in segmented X-ray CT data. Likewise, the small contribution to the overall current density from the passive surface of the wire was also not considered in these calculations.

By only considering the measured X-ray CT data of approach A, the relationship of growth in pit depth over time can be determined, corresponding to $r = a \,.\, t^x$, where (r) represents pit depth, (a) and (x) empirical pit growth constants, and (*t*) time. Computing the pit depths for all 3 pits gives similar values for (x), confirming that pit growth kinetics for all 3 pits were similar. For achieving $t^{0.5}$ a pit growth constant (a) of between 3–5 $\times$ 10^{-6} m.s^{-1} would need to be assumed, which is in the range of typical growth constants reported.[32] This indicates that the pit depth growth rate in 3-D was possibly under diffusion control, similar to the reported $t^{0.5}$ of diffusion control for 1-D[33] and for 2-D[7] pit depths. The 3-D pit lateral growth by assuming *(r)* is the width (w) and height (h), show a relation with time of $>t^{0.5}$. This implies that the width grew in a less than saturated solution faster than the depth, which is also supported by the overall dimensions obtained.

Figure 3b shows a slight variation between pit width and height for pit 1 and 2 compared to pit 3. This indicates that all the pits shape are not hemispherical, with 2-D X-ray CT slices showing an semi-ellipsoid dish shape. The ratio of pit depth over width is in the range of 0.41 and 0.47, fitting well with reported values of 0.4 to 0.5.[13,34]

Current density and stability product.—In order to obtain pit growth rates, the current densities in Figure 4a have been calculated by using the obtained current response of Figure 3a, divided by internal pit surface area. Three values of pit current density over time are presented based on the three approaches A, B and C outlined in Table II.

Figure 4a shows mean current density as a function of time for pit 1. Two regions can be distinguished: the first where the current density increases rapidly and the second where it starts to drop over time. Fluctuations in current density also become smaller over time. The two regions consist of a transient and quasi-steady state period which have been reported for pit growth.[33] The maximum current density of pit 1 reached 5 A.cm^{-2} at the transient region for approach A, reducing to a mean value of 1.8 A.cm^{-2} in the steady state region. Figure 4b shows the results for pit 2 and 3. The behavior of pit current density over time is similar to pit 1, but the time for pit growth was almost doubled. The results also show a limiting current density of 5 A.cm^{-2} for approach A, similar to the maximum value observed for pit 1. At the end of the polarisation scan, a mean current density of 1.3 A.cm^{-2} was estimated.

In Figures 4a and 4b, approach A has the lowest current densities of all three approaches, indicating that the real pit surface area must be larger relative to the assumptions in approach B, with approach C overestimating the pit depth compared to the real pit dimensions (Table II). The difference in current density between approach A and B is nearly 50%, whereas for A and C it is only 6%. An increase of current

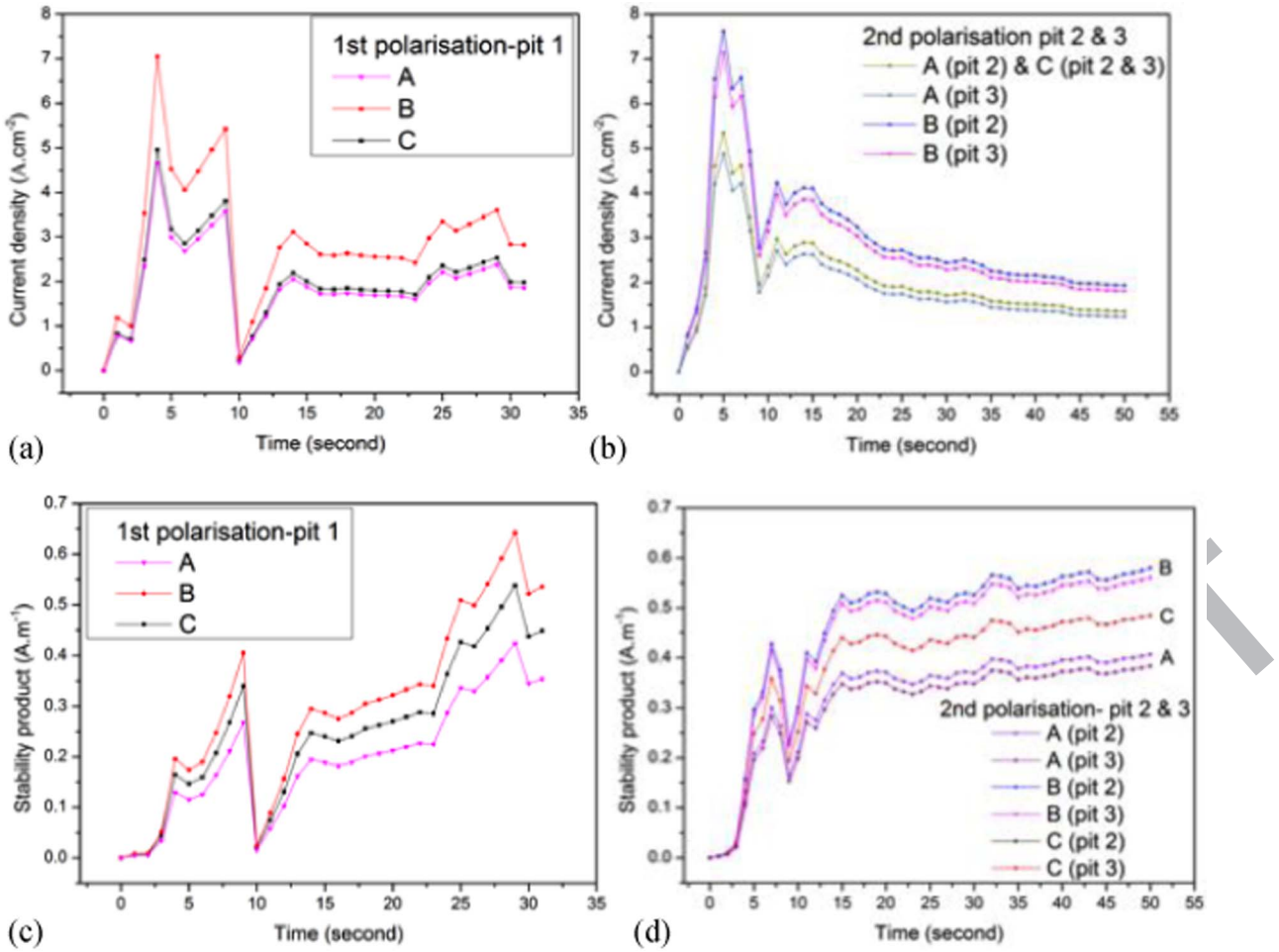

Figure 4. The values in Table II of the three approaches A, B, and C are applied to show (a) pit 1 current density vs. time, (b) pit 2 and 3 current density vs. time, (c) pit stability product vs. time of pit 1, and (d) pit stability products vs. time of pit 2 and 3.

density with increasing polarisation time up to the maximum current value under activation polarisation in the transient stage, and after that the thickness of salt film precipitation affects pit growth.[35] A sharp drop in current density was observed at the transition between both stages, which may indicate that dissolved metals ions reach saturation and salt film precipitation occurs, reducing the measured current at this stage to very low values. Longer pit growth periods clearly show a quasi-steady state of current density. The difference in calculated current density between approach A and approach B and C show that longer pit growth periods in Figure 4b reduce the difference between them to less than 3%.

Figures 4c and 4d show the value of stability products as a function of time for all three pits obtained by the three approaches. Stable pits should have a stability product range of $0.3 < i.r < 0.6$ A.m^{-1}.[12] Pit stability values obtained by the three methods for all pits increased over time, and fit in the range of stable pit criteria. However, the result of approach A relative to approaches B and C show lower stabilities of 25% and 50% respectively. The results also show that pit stability product was initially below the stable pit growth criteria, and then increased with time. At an early stage of pit growth, the pit stability product was below 0.3, and pit growth is then believed to be supported by a diffusion barrier in the form of lacy metal covers.[12] It should be noticed that the above criteria were developed by Pistorius and Burstein for stainless steel in chloride electrolytes, assuming hemispherical open pit growth and 3 M concentration as a minimum for metal ion dissolution for metastable to stable pit transition. The measurement also assumed a diffusion coefficient of $D = 1 \times 10^{-5}$ cm^2.s^{-1}.[12,20]

Comparing the above three approaches in our study, the results indicate that the current density and pit stability product show slight differences. This variation can be related to pit shape differences and the effect of non-uniform dissolution on the local chloride concentration. It appears that using 2-D methods leads to an overestimate in the pit depth growth rate as compared to that obtained from a 3-D analysis of current density and associated stability products.

Pit diffusion product estimations.—Figure 5 shows the relationship between the square of the pit depth (r^2) over time (t) using Equation 1 (derived from Fick's first law and Faraday's second law), which suggests that pit growth with salt layer is under diffusion control. The equation shown below was used to estimate pit diffusion product.[9,12]

$$r^2 = ((3.M.D.\Delta C)/\pi.\rho).t \quad [1]$$

Where, D is the effective diffusion coefficient and ΔC is concentration difference between pit bottom and mouth. The gradients in Figure 5 provide the diffusion product (D.ΔC) with 1.68×10^{-8}, 2.84×10^{-8} and 3.04×10^{-8} mol.cm^{-1}s^{-1} for pits 1, 2 and 3, respectively, by using the pit depths of the segmented volumes in approach A. These show linear relationship between square depth of pits and time, suggesting diffusion controlled pit growth in all cases. The obtained slopes are lower than those reported for diffusion controlled pit growth in 1-D,[7,36] but similar to 2-D pit growth studies facing upward diffusion.[9] Open pit growth in 1-D with pits facing upwards, typical diffusion product values close to 6×10^{-8} mol.cm^{-1}.s^{-1} were obtained in 1 M NaCl solution,[19] whereas, 2-D pit growth in 0.1 M NaCl with pits facing upwards and lacy metal covers showed values similar to our results for

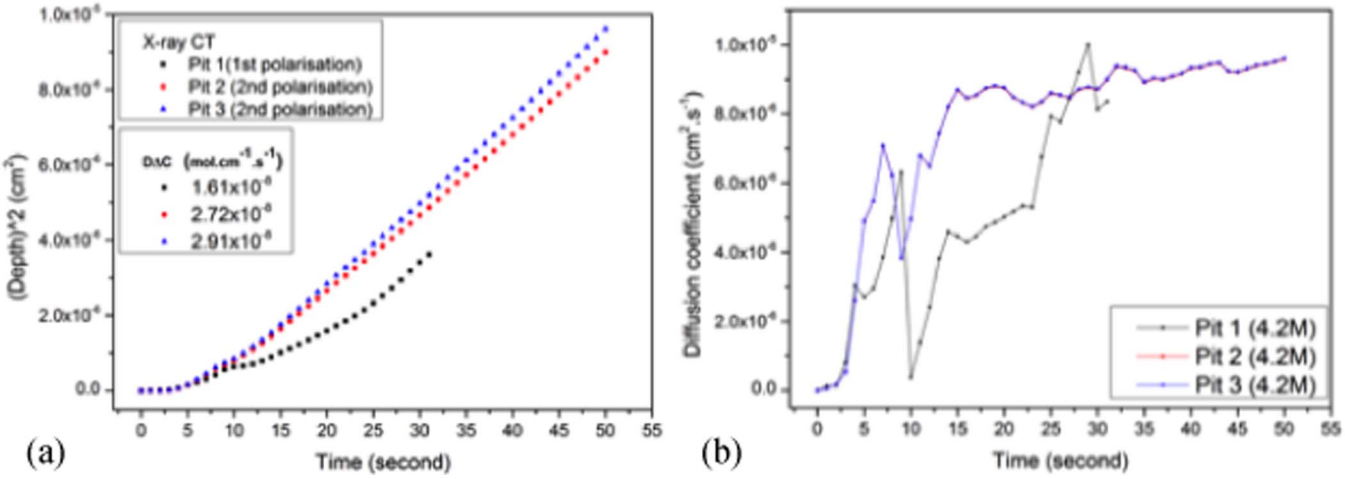

Figure 5. Effect of time on (a) (pit depth)^2 to obtain the diffusion parameters of these curves from the slopes, (b) effective diffusion coefficient (D) estimated with a constant metal ion concentrations of 4.2 M.

pits 2 and 3.[9] It may be possible that 3-D pit growth and vertical sample position allows the electrolyte to be more easily infused by gravity, relative to 1-D and 2-D experimental set-ups, where the electrolyte within the pit is constrained by pit geometry and sample position.[37]

In our study, pit 1 shows a lower diffusion product relative to pits 2 and 3, possibly due to the influence of the lacy cover observed for pits 2 and 3 (Figure 2c), affecting the anolyte concentration inside the pit. A number of factors were suggested to influence the gradient of pit growth, such as the area of perforation of the metal lacy covers, chloride concentration, applied potential, type of electrolyte and temperature, as well as pit growth direction, with respect to the sample position.[7,9,14,19,21,23,38,39] For example, a difference of 15% was reported between pit growth with the sample facing upwards versus downwards in 2-D.[7] In our study, all pits grew vertical at the wire, and minor differences in diffusivity parameters estimated for pits 2 and 3 may even be a result of the difference in perforated area of both pit covers.[9]

If the diffusion coefficient (D) is assumed to be constant at 0.85 $\times$ 10^{-5} $cm^2.s^{-1}$,[9,17] the mean metal salt concentration inside the pits can be estimated from the diffusivity parameters given above. The mean concentration would therefore be around 1.97 M, 3.34 M and 3.57 M for pits 1, 2 and 3, respectively. These values indicate that the mean concentration at the pit bottom for pit 1 is below the 3 M (75% of saturation concentration of $FeCl_2$) suggested for stable growth facing upwards in type 304 stainless steel.[12] It was also suggested that stable pits can propagate without lacy covers, as the pit depth also provides a diffusion barrier to maintain the corrosive solution for active pit dissolution. This would mean that in our case pit 1 propagates without lacy metal cover in 1.97 M metal salt concentration with a pit depth of 19 μm acting as effective diffusion barrier to support stable pit propagation after the pit lost its lacy cover. This concentration is close to the reported values of 1.8–2 M, defined as critical ion concentration for stable pit transition in stainless steel at constant potentials.[40] Furthermore, it is shown that losing the lacy metal cover certainly affects the ion concentrations inside pits, since pit 2 and pit 3 show far higher concentrations of 3.34 M and 3.57 M, respectively, with both growing to similar depths of roughly 30 μm.

However, comparison of the growth kinetics of pits by assuming a constant diffusion coefficient is not correct, since the effect of chloride concentration and its change over time need to be taken into consideration. The effect of chloride concentration can be shown, for example, by assuming a constant metal ion concentration inside the pit of 4.2 M throughout the pit growth period. This would result in our case in mean diffusion coefficients of 0.4 $\times$ 10^{-5} for pit 1, and 0.68–0.72 $\times$ 10^{-5} $cm^2.s^{-1}$ for pits 2 and 3, based on the above diffusivity products of ($D_{,}\Delta C$) 1.68 $\times$ 10^{-8}, 2.84 $\times$ 10^{-8} and 3.04 $\times$ 10^{-8} $mol.cm^{-1}s^{-1}$.

Alternatively, the variation of effective diffusivity (D) with pit growth over time can be estimated using Equation 2,[20] with the results summarised in Figure 5b.

$$\Delta C = (2\pi/(3n.F.D))\ i.r \qquad [2]$$

This gives a realistic approach of the effect of time, by considering (D) as Key variable, and using the evolution of current density (i) and pit depth (r) over time from approach (A) as input parameters. The saturation concentration (ΔC) was kept constant at 4.2 M. Figure 5b clearly shows a large variation of diffusion coefficients during the initial transient stage, which is most likely caused by overestimating the metal ion concentration inside the pit. In reality, lower metal ion concentrations than the one used in this estimation will be present, ultimately resulting in the formation of lacy metal covers.

Interestingly, effective diffusion coefficients of 0.83 $\times$ 10^{-5} for pit 1 and 0.96 $\times$ 10^{-5} $cm^2.s^{-1}$ for pit 2 and 3 are obtained for the steady state pit growth period in Figure 5b, which is close to the estimated diffusion coefficient for 1-D and 2-D pit growth studies.[20,33] The drop of diffusion coefficient between 7–9 second for all pits may indicate salt film precipitation and for pit 1 this may be associated with the time where pit 1 lost its lacy metal cover as seen in Figure 2c.

This study shows that quasi in-situ X-ray CT experiments provide an effective tool to study pit growth kinetics and to probe assumptions for optimising pit kinetics for predicting material behavior. The advantage of the 3-D approach over previous 1-D and 2-D in-situ approaches lies in the reduction of geometrical constraints, by studying real 3D systems. Further experiments are currently conducted with this approach, by inducing nucleation and growth of multiple pits, to understand whether these affect each others growth kinetics, and the influence of strain on pit growth.

Conclusions

1. 3-D pit growth kinetics can be estimated via quasi in-situ measurements from electrochemical polarisation tests with information of pit dimensions using X-ray CT data. The pit volumes obtained by X-ray CT showed good fit with the volume of metal dissolution calculated using Faraday's law.
2. The measured surface area of pits from X-ray CT is larger than those calculated by assuming hemispherical pit growth, with pits approaching elongated dish shapes rather than perfect hemispherical shapes.
3. Typical mean current densities of 1–3 $A.cm^{-2}$ with pit stability product of 0.3–0.6 $A.m^{-1}$ have been estimated for stable pit growth. Diffusivity parameter ($D_{,}\Delta C$) between 1.68–3.04 $\times$ 10^{-8} $mol.cm^{-1}.s^{-1}$ were obtained.

4. Pit growth rates in 3-D indicate that the pit depth is under diffusion control, whilst lateral growth occurred faster.
5. Effective diffusion coefficients (D) from the pit base to the pit mouth were estimated at 0.83×10^{-5} and 0.96×10^{-5} $cm^2.s^{-1}$ for pit growth with assumed metal ion concentrations of 4.2 M.

Acknowledgment

The authors acknowledge the provision of beam time at Henry Moseley X-ray imaging Facility (HMXIF) at the University of Manchester, UK, established with funding from EPSRC through grants EP/F007906, EP/I02249X and EP/F028431. The authors would also like to thank Saline Water Conversion Corporation (SWCC), Saudi Arabia for financial support. Valuable discussions with Dr Anthony Cook (University of Manchester) are also acknowledged.

References

1. G. Frankel, *J Electrochem Soc*, **145**(6), 2186 (1998).
2. Z. Szklarska-Smialowska, *Corrosion*, **27**(6), 223 (1971).
3. T. P. Hoar and W. R. Jacob, *Nature*, **216**(5122), 1299 (1967).
4. N. Sato, *Corrosion Sci.*, **37**(12), 1947 (1995).
5. H. Isaacs and G. Kissel, *J Electrochem Soc*, **119**(12), 1628 (1972).
6. J. Mankowski and Z. Szklarska-Smialowska, *Corrosion Sci.*, **15**(6), 493 (1975).
7. P. Ernst and R. C. Newman, *Corrosion Sci.*, **44**(5), 927 (2002).
8. S. M. Ghahari, A. J. Davenport, T. Rayment, T. Suter, J.-P. Tinnes, C. Padovani, J. A. Hammons, M. Stampanoni, F. Marone, and R. Mokso, *Corrosion Sci.*, **53**(9), 2684 (2011).
9. M. Ghahari, D. Krouse, N. Laycock, T. Rayment, C. Padovani, M. Stampanoni, F. Marone, R. Mokso, and A. J. Davenport, *Corrosion Sci.*, **100** 23 (2015).
10. N. J. Laycock and S. P. White, *J Electrochem Soc*, **148**(7), B264 (2001).
11. N. J. Laycock, S. P. White, J. S. Noh, P. T. Wilson, and R. C. Newman, *J Electrochem Soc*, **145**(4), 1101 (1998).
12. P. C. Pistorius and G. T. Burstein, *Philos T Roy Soc A*, **341**(1662), 531 (1992).
13. R. C. Alkire and K. P. Wong, *Corrosion Sci.*, **28**(4), 411 (1988).
14. N. J. Laycock and R. C. Newman, *Corrosion Sci.*, **39**(10–11), 1771 (1997).
15. R. C. Newman and E. M. Franz, *Corrosion*, **40**(7), 325 (1984).
16. J. González-Sánchez, L. Dzib-Pérez, E. Garcia-Ochoa, G. Canto, and M. Sosa-Baz, *Anti-Corros Method M*, **59**(5), 239 (2012).
17. G. T. Gaudet, W. T. Mo, T. A. Hatton, J. W. Tester, J. Tilly, H. S. Isaacs, and R. C. Newman, *Aiche J*, **32**(6), 949 (1986).
18. U. Steinsmo and H. S. Isaacs, *Corrosion Sci.*, **35**(1–4), 83 (1993).
19. M. H. Moayed and R. C. Newman, *Corrosion Sci.*, **48**(11), 3513 (2006).
20. P. C. Pistorius and G. T. Burstein, *Corrosion Sci.*, **33**(12), 1885 (1992).
21. G. S. Frankel, *Corrosion Sci.*, **30**(12), 1203 (1990).
22. W.-M. Tian, Y.-J. Ai, S.-M. Li, N. Du, and C. Ye, *Acta Metallurgica Sinica (English Letters)*, **28**(4), 430 (2015). Q1
23. W. Tian, S. Li, N. Du, S. Chen, and Q. Wu, *Corrosion Sci.*, **93**(0), 242 (2015).
24. N. Aouina, F. Balbaud-Célérier, F. Huet, S. Joiret, H. Perrot, F. Rouillard, and V. Vivier, *Electrochimica Acta*, **104**(0), 274 (2013).
25. S. M. Ghahari, D. P. Krouse, N. J. Laycock, T. Rayment, C. Padovani, T. Suter, R. Mokso, F. Marone, M. Stampanoni, M. Monir, and A. J. Davenport, *Corros Eng Sci Techn*, **46**(2), 205 (2011).
26. A. B. Cook, D. L. Engelberg, N. P. Stevens, N. J. Laycock, S. White, M. Ghahari, M. Monir, H. J. Holroyd, and R. C. Newman, *ECS Transactions*, **41**(25), 121 (2012).
27. T. Burnett, S. McDonald, A. Gholinia, R. Geurts, M. Janus, T. Slater, S. Haigh, C. Ornek, F. Almuaili, D. Engelberg, and P. J. Withers, *Scientific reports*, **4**, 711 (2014).
28. A. King, G. Johnson, D. Engelberg, W. Ludwig, and J. Marrow, *Science*, **321**(5887), 382 (2008).
29. T. J. Marrow, L. Babout, B. J. Connolly, D. Engelberg, G. Johnson, J. Y. Buffiere, P. J. Withers, and R. C. Newman, in *Environment-Induced Cracking of Materials*, S. A. Shipilov, R. H. Jones, J. M. Olive, and R. B. Rebak, eds., p. 439, Elsevier, Amsterdam, (2008).
30. L. Babout, T. J. Marrow, D. Engelberg, and P. J. Withers, *Mater Sci Tech-Lond*, **22**(9), 1068 (2006).
31. L. Feldkamp, L. Davis, and J. Kress, *JOSA A*, **1**(6), 612 (1984).
32. M. K. Cavanaugh, R. G. Buchheit, and N. Birbilis, *Corrosion Sci.*, **52**(9), 3070 (2010).
33. J. W. Tester and H. S. Isaacs, *J Electrochem Soc*, **122**(11), 1438 (1975).
34. R. K. Ulrich and R. C. Alkire, *Corrosion Sci.*, **23**(11), 1153 (1983).
35. G. S. Frankel, J. O. Dukovic, V. Brusic, B. M. Rush, and C. V. Jahnes, *J Electrochem Soc*, **139**(8), 2196 (1992).
36. M. H. Moayed and R. Newman, *Materials and Corrosion*, **56**(3), 166 (2005).
37. J. Mankowski and Z. Szklarskasmialowska, *Corrosion Sci.*, **17**(9), 725 (1977).
38. H. C. Kuo and D. Landolt, *Electrochimica Acta*, **20**(5), 393 (1975).
39. A. G. Carcea, E. Y. Yip, D. D. He, and R. C. Newman, *J Electrochem Soc*, **158**(6), C215 (2011).
40. N. Sato, *J Electrochem Soc*, **129**(2), 260 (1982).

Query

Q1: AU: Please provide text citation for refs. 22 and 24.